Vol. 6 Issue 2

Meteorology Hydrology and Water Management
Research and Operational Applications

2018

Is there added value of convection-permitting regional climate model simulations for storms over the German Bight and Northern Germany?

Benjamin Schaaf, Frauke Feser

Helmholtz-Zentrum Geesthacht, Max-Planck-Straße 1, 21502 Geesthacht, Germanny, e-mail: benjamin.schaaf@hzg.de

Abstract. This study tackles the question: Do very high-resolution convective-permitting regional climate model (RCM) simulations add value compared to coarser RCM runs for certain extreme weather conditions, namely strong wind and storm situations? Ten strong storm cases of the last two decades were selected and dynamically downscaled with the RCM COSMO-CLM (24 and 2.8 km grid point distance). These cyclones crossed the high-resolution model domain, which encompasses the German Bight, Northern Germany, and parts of the Baltic Sea.

One storm case study (storm Christian of October 2013) is discussed in more detail in order to analyze the small-scale storm features and the associated potential added value of the high-resolution simulation. The results indicate an added value for atmospheric dynamical processes such as convective precipitation or post-frontal cloud cover. The multiple storm analysis revealed added value for the high-resolution regional climate simulation for 10 m wind speed, mean sea level pressure, and total cloud cover for most storms which were examined, but the improvements are small. Wind direction and precipitation were already well simulated by the coarser RCM and the higher resolution could often not add any value for these variables. The analysis showed that the added value is more distinct for the synoptic comparisons than for the multiple storm study analyzed with statistical measures like the Brier Skill Score.

Keywords: case study, wind, very high-resolution, regional climate modeling, added value, storm, cloud-resolving, convection-permitting

Submitted 31 July 2017, **revised** 3 November 2017, **accepted** 20 February 2018

1. Introduction

Severe storms may generate storm surges, flooding, uprooted trees, damage to buildings or high economic losses and therefore have a large impact on coastal populations (Klawa, Ulbrich 2003; Neumayer, Barthel 2011; Pinto et al. 2007). For the North Sea coast, Northern Germany and the city of Hamburg, which is located in close proximity to the coast, winter storms are of general interest since they typically represent the strongest storms in this region. Feser et al. (2015) reviewed a large number of different studies of winter storm activity over the North Atlantic and Northwestern Europe. They found that winter storm activity shows large decadal variability (including a decrease since the 1960s and a subsequent increase for more recent decades) which depends on the analyzed region and time period. However, generally no systematic long-term trends were apparent when looking at the past 100 to 1000 years.

Wind measurements, which are often used to derive storm activity, in many cases suffer from inconsistencies which arise from changes in observation methods, surrounding buildings or trees, or station location. Reanalysis data sets take into account such inhomogeneities of observation data and convert measurements into relatively consistent gridded data sets (which may still be influenced by increasing station density over time and, e.g., the introduction of satellite data) with equal grid spacing and time intervals. These have a relatively low resolution, ranging between about 200 km (for reanalysis of the last more than 6 decades) and 50 km mesh size (for the more recent reanalysis which usually start in 1979 after the introduction of satellite data). Weisse et al. (2005, 2009, 2014) analyzed the long-term change of storminess in Europe by dynamically downscaling reanalysis data with regional climate models (RCMs). The usage of RCMs forced by reanalysis data at its lateral boundaries can help to minimize potential inhomogeneities in reanalysis and achieve higher resolutions. This approach was also applied in the current study, which dynamically downscales a RCM simulation forced by reanalysis data to a convective-permitting resolution.

The added value of RCMs in comparison to coarser model data sets like reanalyses was determined in numerous studies in regional climate hindcasts. For instance, Feser et al. (2011) describe added value for several studies over Europe in numerous variables and areas. The potential for added value in RCMs and for dynamical downscaling was investigated by Di Luca et al. (2012, 2015). The potential added value describes small spatial scale variability in regional climate statistics which could

not be simulated on coarser grids as a prerequisite for added value. They found that a more meaningful added value may be found by exploring conditions conducive to particular weather and climate events than by focusing on simple statistics and that the potential added value of RCMs is much higher for short time scales (e.g. hourly data) than for long time scales (monthly mean). An RCM ensemble study by Di Luca et al. (2016) showed the strong dependence of added value on the type of driving data, the variable, and the region of interest. An added value for RCM simulations was found mainly due to a more detailed spatial variability of surface variables as, for instance, the 2 m temperature in coastal areas or regions with structured topography. Li et al. (2016) investigated the added value of an RCM using satellite and in situ observations as references for the region of the Bohai Sea and Yellow Sea and found an added value especially in coastal regions. Winterfeldt and Weisse (2009) discussed the added value of an RCM with a resolution of 50 km for a time period of 10 years (1994-2003) and showed an added value for RCM wind speed compared with reanalyses (they also used satellite data as a reference). They found an added value for areas with more structured orography and coastal regions, but not over the open sea and the German Bight.

High-resolution RCMs are usually nested into a coarser RCM simulation, which is driven either by general circulation models or by reanalysis data. These high-resolution RCMs are expected to show an added value over their large-scale forcing data at the regional scale. This may be a more realistic simulation of convection or of other meteorological small-scale effects like wind flow dominated by topography (Cholette et al. 2015). The horizontal grid distance of a convection-permitting simulation should be smaller than 4 km to resolve explicitly convective processes like precipitation or convective gusts, so that parametrizations for subgrid processes are no longer necessary (Prein et al. 2015). Comprehensive studies of the current state of high-resolution climate models and their potential added value were carried out by Parker et al. (2015) and Prein et al. (2015). They found that convective-permitting RCMs show improvements for deep convection, mountain regions and extreme events. Most studies using convective-permitting RCMs currently concentrate on the added value of precipitation as this variable is most promising with regard to providing a benefit at this high resolution. For instance, Prein et al. (2013) analyzed the added value of an ensemble of convective-permitting seasonal simulations in comparison to coarser grid RCM simulations over the European Alps for temperature, precipitation, relative humidity and radiation. They reported an added value for summertime precipitation diurnal cycles, extreme precipitation intensities, and a more accurate distribution of rain. Chan et al. (2014) compared a 1.5 km RCM to a 12 km simulation for the southern United Kingdom from 1990 to 2008. They presented added value for precipitation extremes for the 1.5 km RCM simulation, especially for summer. They also showed that the high-resolution run could also realistically simulate the dynamical structure and life cycle of convective storms (Chan et al. 2014).

There have only been a few dynamical downscaling studies so far showing the added value for storms, and most of these cover tropical cyclones. Xue et al. (2013) analyzed the Atlantic hurricane season of 2010 with an RCM using a 4 km grid by means of 48 h TC forecasts. The high-resolution RCM showed benefits in comparison to its global forcing data for forecasted TC tracks and TC intensity, with the largest improvements for TCs that feature hurricane strengths. Gentry and Lackmann (2010) studied hurricane Ivan of 2004 in an RCM with varying grid sizes between 8 and 1 km. The higher resolutions resulted in an increase in storm intensity and a broader range of updraft and downdraft processes in the eye wall. Taraphdar et al. (2014) analyzed TCs over the Indian Ocean in high-resolution weather forecasts computed with RCMs at 10 and 1.1 km resolution. They found that the high-resolution simulations lead to modelled TC tracks and intensities which were closer to observations than the simulations which used parameterized convection. But the higher resolution had no effect on the intrinsic predictability limit, which was the same for both simulations.

So far, there are only a small number of studies which examine extra-tropical cyclones in high-resolution models. Most of these did not look into the added value of convection-permitting simulations in comparison to coarser RCM or GCM simulations. For instance, Gallagher et al. (2016) dynamically downscaled wind and waves from ERA-Interim reanalysis with a meso-scale model of 2.5 km grid size. The authors assessed the uncertainty regarding the wind and wave renewable energy potential in Irish coastal areas with this 14-year hindcast from 2000 to 2013. The data set's quality for wind and waves was found to be good in comparison to observations. Ludwig et al. (2015) analyzed the formation of a secondary cyclone along the occluded front and severe cold front of storm Kyrill of January 2007. The high-resolution RCM run realistically reproduced observed storm features and the gusts along the cold front were often close to observations and exceeded hurricane strength. Other extra-tropical winter storms were investigated in RCM studies, such as Anatol (Nilsson et al. 2007), Lothar and Vivian (Usbeck et al. 2012), and Xynthia (Liberato et al. 2013). These studies showed that an RCM with a high resolu-

Tab. 1. Analysis period and number of hourly values used for the calculation of the BSS for each of the ten storm events investigated

Storm name	Analysis period	Number of values for BSS
Anatol	3-4/12/1999	48
Kyrill	18-19/01/2007	48
Emma	29/2-2/3/2008	72
Xynthia	28/2-2/3/2010	72
Yoda	26-28/11/2011	72
Christian	28-29/10/2013	48
Xaver	4-7/12/2013	96
Anne	3-4/1/2014	48
Gonzalo	21-22/10/2014	48
Niklas	31/3-2/4/2015	72

tion of 2 km produces a realistic wind field compared with observations. Some case studies on the added value of RCMs running in numerical weather prediction mode have been published (e.g. Kain et al. 2006; Baldauf et al. 2011). The majority of these focused on precipitation as this variable is most likely to add value in convection-permitting simulations.

In this work we analyze the added value of high-resolution convection-permitting regional climate simulations for ten strong extra-tropical storm cases over the North Sea, the German Bight, and Northern Germany. The storms of interest are listed in Tab. 1. This study is the first to analyze the added value of convection-permitting RCMs with a focus on very high wind and storm conditions. We here compare two RCM simulations with different resolutions against reference measurement data using different statistical measures. The article is structured as follows: in Chapter 2 we introduce the model configuration, the model domain and the data used for comparisons. The results of a detailed analysis of the storm Christian are presented in Chapter 3.1. In Chapter 3.2 the analysis and added value of the high-resolution simulation for all storm events investigated are shown. Finally, the summary and conclusions are given in Chapter 4.

2. Model configuration, data, and methods

2.1. Model configuration

The COSMO model is a non-hydrostatic limited-area atmospheric prediction model from the German weather service (DWD). For this study the model COSMO-CLM (Steppeler et al. 2003; Rockel et al. 2008) (CCLM), which is the climate version of the COSMO model, version 5.0 was used. Two different CCLM simulations will be compared to each other, one with a grid distance of about 24 km (CCLM240) and one with a grid distance of about 2.8 km (CCLM028). Both model domains are shown in Fig. 1. The coarse simulation is the CoastDat II data set (hereinafter referred to as CCLM240), which is an atmospheric hindcast for Europe for the last 67 years, from 1948 to 2015 (Geyer, Rockel 2013; Geyer 2014). For the CCLM240 simulation the CCLM model (version 4.8) was applied. It has a spatial grid distance of 0.22° (about 24 km), 234×228 grid points, 40 layers up to 27.2 km height in the vertical, 10 soil levels down to 11.5 m depth, a rotated pole at 170.0°W and 35.0°N, and a time step of 150 seconds. CCLM240 is driven by the NCEP1 (grid distance 1.875°) reanalysis data set (Kalnay et al. 1996). In the following, the high-resolution storm simulations will be referred to as CCLM028. The model domain covers the German Bight and the western part of the Baltic Sea (Fig. 1) with a spatial grid distance of 0.025° (about 2.8 km), 250×180 grid points, 40 layers in the vertical, a rotated pole at 8.82° E and 54.45° N, and a time step of 25 seconds. The lateral sponge zone has a width of 12 grid points, so we analyzed 226×156 grid points in this study. The climate simulation is forced by CCLM240. The double nested hindcast simulation CCLM028 (from NCEP1 to CCLM240 and from CCLM240 to CCLM028) was computed for ten individual storm cases in climate mode, which means that the simulation is continuous for the whole storm event and no repeated initialization is carried out during the model run. For each storm, the preceding month was computed for the spin-up of the model, followed by the month the storm evolution took place. The most relevant atmospheric variables for this study, such as wind speed, pressure, or precipitation, are stored with hourly resolution.

The spectral nudging (SN) technique described by von Storch et al. (2000) was applied for the CCLM240 simulation to keep large weather systems (larger than about 1200 km) close to the large-scale atmospheric conditions simulated by the forcing reanalysis. Smaller spatial scales were not nudged; these were solely computed by the regional climate model. Only the horizontal wind components (U, V) were spectrally nudged towards the reanalysis. The influence of SN increases exponentially from 850 hPa to the top of the model domain. Below 850 hPa no SN is applied, so that small weather phenomena, which often occur close to the surface, are not affected. Test simulations, which are referred to the 2.8 km simulation, with and without SN showed no significant differences and therefore lead to the conclusion that spectral nudging is not necessary for high-resolution simulation. This is presumably a consequence of the relatively small model domain as spacious weather patterns which deviate from observed large weather systems have no time to develop

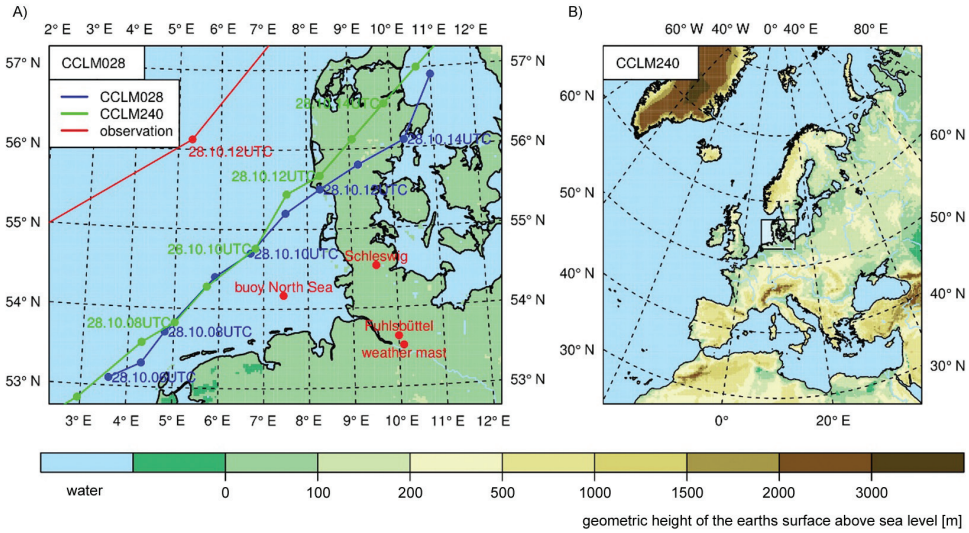

Fig. 1. Model domain of a) the high-resolution simulation CCLM028 and b) CCLM240 and related topographies; the locations of the weather stations used for most comparisons in the study are shown as red dots; storm tracks of storm Christian of CCLM028 (blue), CCLM240 (green) and the German Weather Service (DWD) analysis (red) are shown as well

inside this domain (Schaaf et al. 2017). In addition, the area of the German Bight is topographically very flat and often dominated by strong westerlies and this prevailing exchange of air masses between the model boundaries and its interior leads to a smaller potential effect of SN. Due to the high resolution, many meteorological phenomena such as convective clouds can be simulated explicitly by the model. The model implies two convection types. One type is deep convection, which describes thermally driven turbulent mixing with vertical motion throughout large parts of the troposphere (above the 500 hPa level) producing precipitation. The other type is shallow convection with limited vertical mixing such as cumulus clouds, which does not generate precipitation. CCLM240 uses both convection parameterizations. CCLM028 uses a grid point distance of 2.8 km and can thus simulate precipitating deep convection explicitly (Prein et al. 2015). Therefore, the CCLM028 simulation only uses the shallow convection scheme, which is a simplified Tiedtke scheme (Tiedtke 1989). It incorporates a number of simplified assumptions, e.g., on the convection vertical extent, and neglects dynamic entrainment, meaning that no precipitation is produced by the parameterization. The friction velocity was parametrized after Schulz and Heise (2003) and Schulz (2008).

The CCLM028 and CCLM240 simulations differ in their horizontal resolutions and their convection schemes, which leads to the following distinctions: The high-resolution CCLM028 simulations feature about 70 grid points in comparison to each coarser CCLM240 grid point and can thus simulate much more detail, e.g., small islands like the North Frisian Islands of Amrum or Föhr can be resolved. Also, the roughness length shows more detail for CCLM028, whereby the range of the roughness length is larger than in CCLM240, and places with higher roughness (e.g. cities) appear much more clearly. A further difference is the time step of the simulations, which decreases from about 5 minutes for CCLM240 to 25 seconds for CCLM028. The main dynamical difference between the two simulations is the ability of CCLM028 to resolve small convective clouds and associated weather features explicitly. The 2.8 km simulation can develop vertical dynamics, which cannot be developed by the coarser simulation. Hence we expect small-scale variables like precipitation or wind speed to show more details and thus potential added value. Also, the more detailed coastline in the high resolution simulation may lead to more realistic results.

2.2. Data

For comparisons with the observations, data from the Wettermast (weather mast) weather station in Hamburg (Lange 2014) in Northern Germany was used. The weather mast measures the wind speed up to 280 m with six platforms at height levels 50, 70, 110, 175, 250, and 280 m. On each platform there is a south-oriented arm that holds the measuring instruments. There is a separate mast with a height of 10 m, which measures all variables at this height. For all other comparisons with observations we used data from 115 observation stations of the German Weather Service[1] located in the CCLM028 model domain, and which provide hourly data. Wind speed and wind direction in 10 m, precipitation, sea level pressure and total cloud cover were compared to model data. A distance-weighted

[1] WebWerdis (http://www.dwd.de/webwerdis)

average of the four nearest neighbor grid point values was used for each model value.

The analyzed track data for storm Christian were provided by the German weather service (von Storch et al. 2014). The satellite data used for comparison were taken from NOAA and METEOSAT[2]. 12-hourly sounding measurements at the observation station Schleswig in Northern Germany served as a reference for simulated vertical wind profiles. The data were provided by the University of Wyoming[3].

2.3. Methods

This study focuses on the added value of very high-resolution RCM simulations for storm situations. Hereby, we define the added value of convective-permitting simulations in comparison to coarser RCM simulations divided into potential added value (prerequisites for added value exist, but added value remains to be shown) and added value can be demonstrated as described in the following:

Potential added value:

- higher spatial resolution and more complex roughness length;
- more detailed coastlines or orography;
- more abundant and varying vegetation and soil characteristics;
- simulation of very small-scale dynamical atmospheric processes.

Added value:

- more realistic high-resolution atmospheric features and patterns in comparison to e.g. satellite data or vertical sounding data;
- smaller bias/*RMSE* compared to observations;
- positive Brier Skill Score, which serves as a measure of simulation quality;
- positive sign test over statistical measure at a station in comparison to observations;
- percentile distributions closer to measurements.

The Brier Skill Score (*BSS*; von Storch, Zwiers 2002) was used to test which of the two RCM simulations provides a more realistic representation of various meteorological variables in comparison to measurement data. It represents a measure of quality for comparing two simulations against each other with measurement data serving as a reference. In this study the modified BSS after Winterfeldt et al. (2010) was used, which is given by:

$$BSS = \begin{cases} 1 - \sigma^2_{\mathrm{CCLM028}}\ \sigma^{-2}_{\mathrm{CCLM240}} & \sigma^2_{\mathrm{CCLM028}} \le \sigma^2_{\mathrm{CCLM240}} \\ \sigma^2_{\mathrm{CCLM240}}\ \sigma^{-2}_{\mathrm{CCLM028}} - 1 & \sigma^2_{\mathrm{CCLM028}} > \sigma^2_{\mathrm{CCLM240}} \end{cases} \quad (1)$$

where: $\sigma^2_{\mathrm{CCLM028}}$ and $\sigma^{-2}_{\mathrm{CCLM240}}$ represent the error variance of the CCLM028 and the CCLM240 simulations. The error variance is the square error of the modelled variable compared to the observation. The *BSS* can vary between –1 and +1. Positive values represent a better performance of the high-resolution simulation CCLM028. Negative values represent a better performance of the coarse-resolution simulation CCLM240 in comparison to measurement data. The error variances for both RCM runs are computed with DWD measurement data serving as a reference.

To merge different *BSS*s, a sign test (von Storch, Zwiers 2002) was used, in this case the two-sample problem was avoided. The sign test counts how often the *BSS* is positive or negative for a station, storm, or variable. Here, we use the sign test to merge the *BSS*s for either all available stations for each storm and variable individually or to merge the *BSS*s for all storms at each station and for all variables. Subsequently the probability *P* that the *BSS*s are positive in at least k cases at a certain station was calculated by:

$$P = \sum_{n \ge k} \frac{m!}{n!\,(m-n)!} 0.5^m \quad (2)$$

where: *m* represents the number of storm events which are considered, *n* represents the number of storm events with positive *BSS*s, and *k* is the number of storm events with positive *BSS*s at the respective station. This probability determines the level of significance. The significance was calculated for all storm events merged at each station. The application of this test for all stations merged for each storm is not possible because the stations are not independent of one another.

Another index which is used to show an added value is the root mean square error (*RMSE*). The *RMSE* is given by:

$$RMSE = \sqrt{\frac{1}{n} \sum_{i=1}^{n} (x_i - y_i)^2} \quad (3)$$

where *x* and *y* are the observed and modelled variables. The *BSS* is the ratio of the *RMSE* of the CCLM028 and the CCLM240 simulations. For the calculation of the *BSS* and *RMSE* hourly measurement data and RCM output data were used for the duration of each storm event.

For the investigation of the potential added value of the convective-permitting RCM simulations ten important high-impact storms over Northern Germany of the last 20 years were examined. Table 1 lists all ten storm events and the time period the CCLM028 model domain was affected

[2] NOAA/METEOSAT, Satellite data, (http://imkhp2.physik.uni-karlsruhe.de/~muehr/archive.html)

[3] Sounding data (http://weather.uwyo.edu/upperair/sounding.html)

by the storm. The number of hourly values, which are used for the calculation of the *BSS*, varies between 48 and 96 for the different storm events. The model domain of the high-resolution simulation CCLM028 is not large enough to capture the entire development of all investigated storm cases. The incorporation of the storm origin regions may result in an improved storm representation as the storms would have more time to develop inside the model domain at high resolution, featuring presumably more realistic dynamical processes. But to include all 10 storm origins which were analyzed in this study, we would have to enlarge the model domain to a size about as large as the CCLM240 domain. This would increase the computing time enormously. In addition, such a large model domain would request the use of spectral nudging, which also increases the computing time by about 15%, to keep larger weather phenomena close to observations as the model would otherwise tend to simulate alternative weather states for certain weather situations (especially those with little exchange via the lateral boundaries, e.g., von Storch et al. 2000). But due to the limited model domain of CCLM028, the storm tracks are close to observations even though no spectral nudging was applied.

The simulated storms analyzed in this study were tracked with a simple tracking algorithm (Feser, Storch 2008) on the basis of sea level pressure and near-surface wind speed. For the tracking, the sea level pressure fields were digitally filtered (Feser, von Storch 2005) so that only the spatial scales of interest (370 km to 100 km) remained. In the first step, sea level pressure minima were detected, which were then combined to tracks according to different selection criteria like minimum track length, wind speed threshold, or maximum storm travel distance between two time steps.

3. Results

3.1. Storm Christian

In the following chapter we look at a single storm in more detail in order to show differences in the regional-scale storm dynamics and associated atmospheric patterns between the coarse and the high-resolution RCM simulations.

3.1.1. Storm development

Storm Christian of October 2013 was chosen because it was a very fast moving low pressure system and also a very intense storm. It led to large amounts of damage due to its early occurrence in the year, which meant that many still densely foliated trees were blown over (Haeseler, Lefebvre 2013). The storm featured high wind gusts and caused a lot of damage, especially in the area of the model domain. Storm Christian formed on the 26th of October 2013 over the Western Atlantic off the Northeastern coast of the US. It moved along the southern coast of England and the North Sea, crossed Denmark where it reached its maximum intensity (von Storch et al. 2014), and then headed across Sweden and the Baltic Sea towards Finland and Russia. Christian was a low pressure system which proceeded with a forward speed of 1200 km in 12 hours (Haeseler, Lefebvre 2013). It was a so-called Shapiro-Keyser-cyclone, named after the cyclone model of Shapiro and Keyser (1990). Such a cyclone does not show much of a classic occlusion like normal low pressure systems. Instead, the cold front is weaker, intersects the warm front at a right angle, and the warm air is located close to the low pressure center.

3.1.2. Added value of the high-resolution simulation in comparison with CCLM240 for storm Christian

Storm Christian was tracked as described in Chapter 2.2. The storm tracks represented in the CCLM240 and the CCLM028 simulations (Fig. 1a, blue and green lines) show a more southerly position (about 150 km) than the track deduced from a sea level pressure analysis performed by the DWD (Fig. 1a, red line). The modelled storms move slightly faster than the one derived from observations. Figure 2 shows the precipitation rate, pressure field and wind speed on October 28, 2013, at 12 UTC. The cold front passes the model area between 9 and 15 UTC. In the 2.8 km simulation (Fig. 2a), the cold front can be detected by an increased precipitation rate and a 'nose' in the pressure field. This 'nose' is typical for a cold front, which results from a rapid increase in pressure behind the cold front. In the CCLM240 simulation (Fig. 2b), these features cannot be seen. But both simulations show a change in wind direction. Other high-resolution details of the CCLM028 simulation are clear weather spots behind the cold front caused by small-scale dynamical processes. The ceilometer backscatter intensity for storm Christian (Fig. 3) at the Hamburg weather mast station (see Fig. 1) shows clear patches behind the cold front (total cloud cover of 30%). These are visible in the simulated total cloud cover of the CCLM028 simulation Fig. 4a, c), but not in the CCLM240 data set (Fig. 4b, d). A satellite image[4] (Fig. 4e) of October 28, 2013, 13 UTC, confirms the cloud-free area behind the cold front. This feature can also

[4] NOAA/METEOSAT, satellite data (http://imkhp2.physik.uni-karlsruhe.de/~muehr/archive.html)

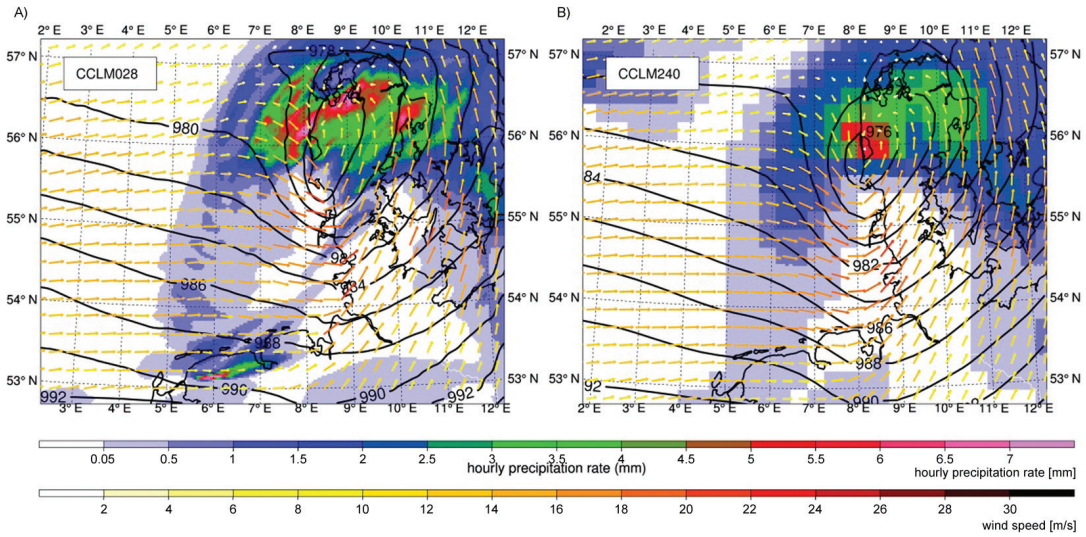

Fig. 2. Precipitation rate (shaded areas) in combination with wind vectors and isobars (black lines) for storm Christian on October 28, 2013, 12 UTC; a) CCLM028, b) CCLM240

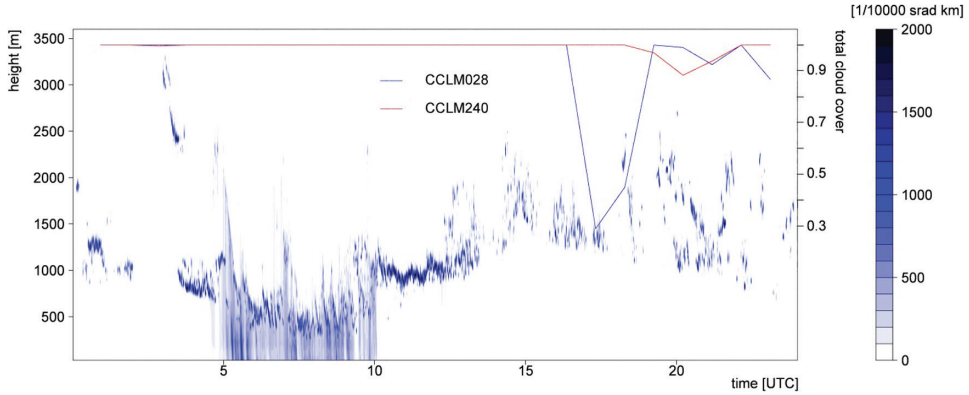

Fig. 3. Ceilometer backscatter intensity at Hamburg weather mast (see Fig. 1) for storm Christian on October 28, 2013, 00 UTC – October 29, 2013 00 UTC in 1/10000 srad km; the lines represent the time series of total cloud cover at weather mast Hamburg (see Fig. 1) for CCLM240 (red) and CCLM028 (blue)

be seen in Fig. 4a-d, which show the total cloud cover for the entire model domain at 13 and 14 UTC. Again, the areas of clear and partly cloudy skies were only simulated by the 2.8 km simulation.

Another interesting feature of the storm is the post-frontal subsidence. Directly behind the cold front strong downward motions dominate, before typical convective motions arise, which leads to cumulus clouds and some scattered showers. The area of the post-frontal subsidence moving eastwards is clearly visible in Fig. 4 for CCLM028 as well as in the satellite images (Fig. 4e). In Figure 4c there are cloud free areas at the North Sea coast and a clear sky band over the south east part of Hamburg (white colors) with a cloud cover between 0% and 20%, which are not present at the same time in the CCLM240 simulation (Fig. 4d). Also the satellite image shows these spots with a quite similar structure. Cloud free spots over the North Sea and along the Coast and the clear sky band over Hamburg is visible in Fig. 4e, which can be identified by green colors over land and white colors over sea in this case. Since the low pressure system is slightly faster in the model simulations than in the analysis of the German weather service, the cold front and the highest wind speeds cross the city of Hamburg more than two hours earlier in the simulations compared to the observations. The vertical wind profile at the location of the Hamburg weather mast, depicted in Fig. 5, shows the maximum wind speed during the intense phase of storm Christian on the 28th of October, 2013, which means that the values can come from different times between 00 UTC and 23 UTC. The simulated maximum wind speeds are underestimated in comparison to the measured ones. But on the contrary, for most time steps, the modelled wind speed of both simulations is overestimated in comparison to the 10 m Hamburg weather mast observations.

Figure 5 represents the vertical wind profile at the station Schleswig on the 28th of October 2013, 12 UTC, for all model levels up to 22 km. Upper air sounding measurements serve as a comparison. The simulations are in good agreement with the vertical profiles of the sounding

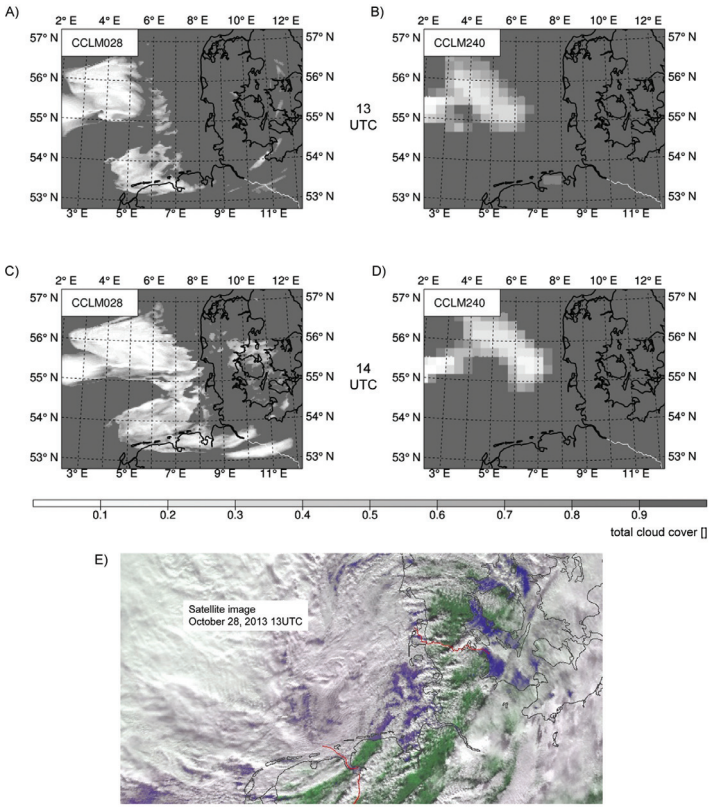

Fig. 4. Total cloud cover for storm Christian on October 28, 2013, 13 and 14 UTC for CCLM028 (a, c) and CCLM240 (b, d) at 13 (a, b), 14 (c, d); grey shows a high backscatter signal and consequently clouds or precipitation; white areas represent cloud-free skies; satellite image of October 28, 2013, 13 UTC © DLR (e); white represents clouds, green represents visible land areas and blue represents visible sea areas; this means that areas with blue and green have cloud-free skies

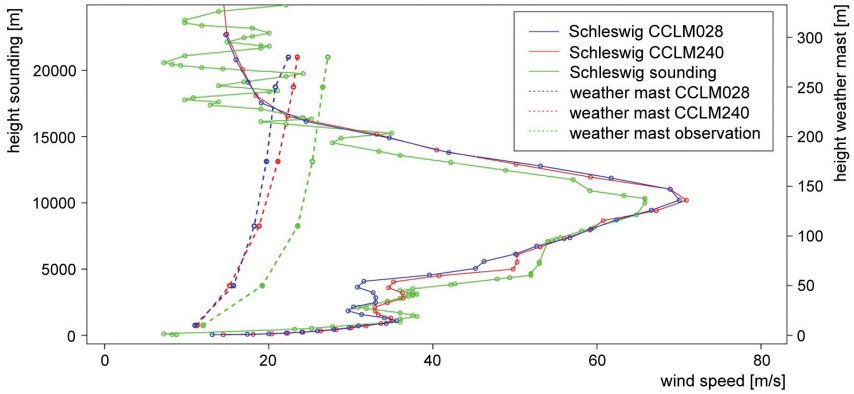

Fig. 5. Vertical wind profile at the Schleswig station in Northern Germany (see Fig. 1a) for CCLM240 (red) and CCLM028 (blue) compared with sounding measurements (green) on the 28th of October 2013 at 12 UTC (solid lines); vertical wind profile at weather mast Hamburg in CCLM240 (red) and CCLM028 (blue) in comparison with the weather mast Hamburg measurements (green, for its location see Fig. 1a) for the maximum mean wind speed during storm Christian on the 28th of October, 2013 (dashed lines)

measurements. Figure 6 shows sea level pressure and 10 m wind speed at the Hamburg airport meteorological weather station. The measurements show lower pressure values than the simulations, but the temporal evolution is very similar. The highest wind speeds occur shortly after the cold front passage which is marked by a sea level pressure minimum. The wind speed peaks on the 28th of October 2013 (12 UTC to 15 UTC) are visible in both simulations, but in the simulations the front passes Hamburg about 2 hours earlier than in the observations.

Finally, the *BSS* for storm Christian between CCLM028 and CCLM240 in comparison to DWD station data was computed at all available stations for the variables wind speed, wind direction, total cloud cover, mean sea level pressure, and total precipitation (Fig. 7). Green indicates positive *BSS*s and thus an added value for CCLM028 compared with CCLM240. Negative *BSS* values (added value for CCLM240) are plotted in orange to red, white dots show *BSS* values around 0 (indicating a similar quality for CCLM028 and CCLM240), and black dots represent

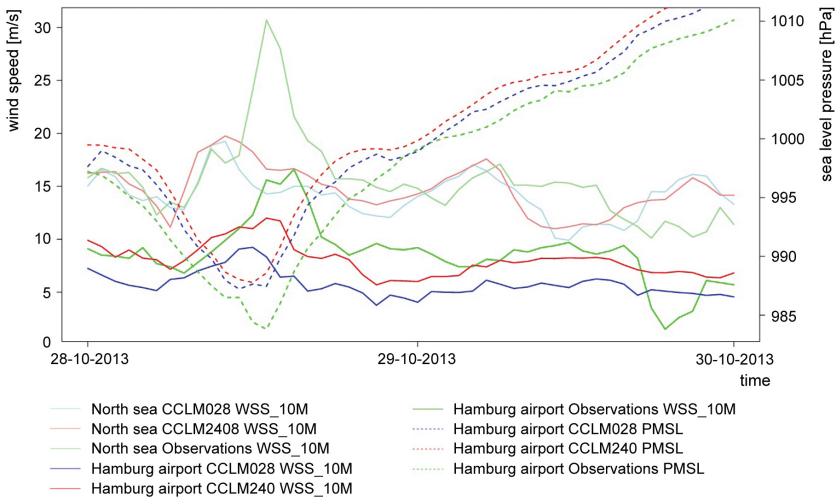

Fig. 6. Time series of storm Christian in CCLM240 (red), CCLM028 (blue) and observations (green) for the Hamburg airport station (strong colours) in Northern Germany (see Fig. 1a) and for a buoy in the North Sea (light colours); shown is 10 m wind speed (solid lines) and sea level pressure (dotted lines)

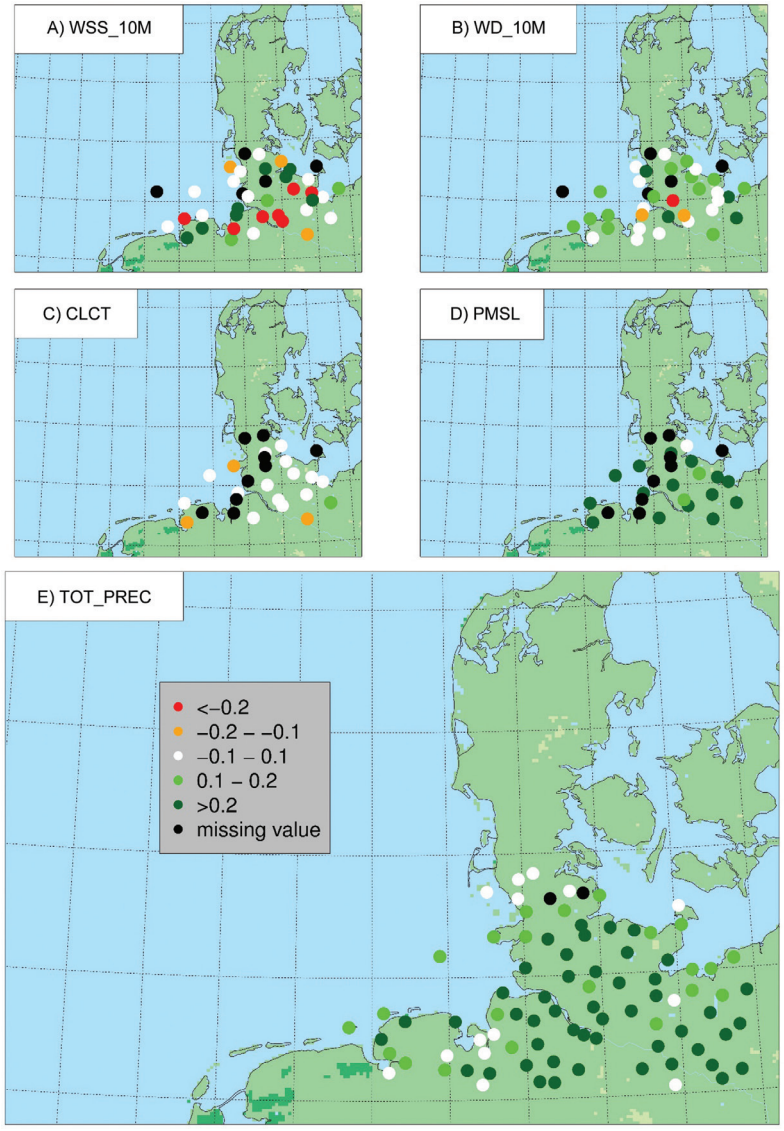

Fig. 7. Brier Skill Score between CCLM028 and CCLM240 in comparison to DWD station data for storm Christian at all available DWD stations for the variables: a) wind speed (WSS), b) wind direction (WD), c) total cloud cover (CLCT), d) mean sea level pressure (PMSL), and e) total precipitation (TOT_PREC); *BSS* values larger than 0 (green) indicate an added value for CCLM028 compared with CCLM240; negative *BSS* values (added value for CCLM240) are plotted in orange to red; white dots show *BSS* values around 0 (CCLM028 and CCLM240 have similar quality) and black dots represent missing values

Tab. 2. Number of stations which show a positive or negative *BSS*, corresponding to Fig. 7

	Positive *BSS*	Negative *BSS*
WSS	15	18
WD	22	11
CLCT	7	11
PMSL	18	0
TOT_PREC	80	4

missing values. The numbers of stations with positive, negative or zero value *BSS*s are given in Tab. 2. For storm Christian, the largest added value is found for mean sea level pressure and precipitation. The *BSS* is positive at almost all stations (no negative values) and thus indicates an added value for CCLM028 for these variables. A weak added value is apparent for wind direction, while for total cloud cover and wind speed both RCMs are of about the same quality. However, the values of the improvements described by the *BSS* are generally small. Therefore the added value shown for the synoptic comparisons like the improved precipitation at the cold front or the improved postfrontal subsidence is more important.

3.2. Multiple storm analysis

3.2.1. Added value for all storms and observation stations

In this chapter we analyze the added value of the high-resolution RCM simulations in comparison to measurement data for ten storm cases described above. *BSS*s were computed between CCLM028 and CCLM240 in comparison to DWD station data for all storm cases at each station available for five variables: wind speed, wind direction, total cloud cover, mean sea level pressure, and total precipitation. Further, a sign test (see Chapter 2.3) was computed which counts how often the *BSS* is positive or negative for all storms available at each station. Figure 8 shows the percentage of storm cases with a *BSS* larger than 0, which indicates – as green dots – an overall added value of CCLM028 compared with CCLM240. White dots represent a value of 50% for the sign test (the same quality for CCLM028 and CCLM240), while red dots show values smaller than 50% (CCLM240 performs better in comparison to observations). The numbers in the dots give the percentage of positive *BSS* values. For several storm events and variables, station measurements were not available, so the total number of stations varies between the individual sign tests.

In addition, a significance test was performed. It tested at each station if the number of storms that did add value for either CCLM028 or CCLM240 was significant or not. We would like to emphasize that such a test of significance may be problematic as the individual stations taken into account cannot be regarded as being independent due to their close proximity. In Figure 8 very light colours show stations where the sign test was not significant at the 10% significance level (SL) according to the significance test. Medium-light colours represent results which are significant at the 10% SL, but not at the 5% SL. Dark colours show a SL of 5%. In addition to the usual 5% SL, the 10% SL was introduced because even with 10 different storm events it is hard to achieve an SL of 5%. It is quite rare that a station can provide hourly measurements for the entire duration of all storm cases. Even if this is the case, to reach the 5% SL, 9 out of 10 cases have to achieve a positive sign test. If a certain station can only provide measurements for, say, 7 storm cases, then a positive sign test is needed for every single storm in order to reach the 5% SL. Table 3 shows the number of stations which feature either a positive, negative, or neutral sign test.

Tab. 3. Number of stations which show a positive, neutral, or negative sign test (with 5%, 10%, or no significance), corresponding to Fig. 8; the positive/negative sign test is defined as a positive *BSS* for more/less than 50% of all storm cases available at a station

Significance	Positive sign test			Neutral sign test	Negative sign test		
	5%	10%	none	none	5%	10%	none
WSS	9	4	24	5	6	0	12
WD	7	2	31	9	3	0	8
CLCT	0	5	15	3	3	0	1
PMSL	8	6	13	0	0	0	0
TOT_PREC	11	17	44	6	13	2	10

For wind speed the sign test is positive for most stations and thus shows an added value for CCLM028. But the values are all small. For wind direction, most stations do show a positive sign test, but the majority of these are not significant. The total cloud cover again features a positive sign test at most stations, with many of these not being significant. Here, only few stations right at the coast and the station on the island of Heligoland show a negative sign test. For mean sea level pressure, the sign test is positive for all stations, but again the values are small. For precipitation, which has the highest station data coverage, most coastal stations return a positive sign test, while many stations located further inland show negative values. The reason for this result is unknown, but most stations with a negative sign are located close to the lateral boundaries and are right next to the model's sponge zone, which may have had an effect, although the sponge zone was already cut off for the analysis. Even though the large majority of stations did show added value for CCLM028

precipitation, the overall values are small and most of these are not significant, thus only for the significant ones an added value for CCLM240 results. In short, sea level pressure and 10 m wind speed show the added value with the highest significance rate. Total precipitation, total cloud cover and wind direction also show an added value for the high resolution simulation, but the SL is lower than 10% for most of the stations.

After comparing all storms at each station, we now analyze atmospheric variables at all stations for each individual storm event. Figure 9 shows a bar plot of the ratio of stations with a positive *BSS* and smaller *RMSE* for CCLM028 for all storm cases and the variables of wind speed, wind direction, precipitation, mean sea level pressure, and total cloud cover. For all variables, the *BSS* returns an overall added value for CCLM028. Similar to the sign test at the different stations, the mean sea level pressure shows the most positive result, followed by wind direction, and then wind speed, total cloud cover, and precipitation. The *RMSE* shows similar results for sea level pressure and wind direction, but for precipitation, wind speed and cloud cover there is no clear added value.

Figure 10 shows the mean percentile-percentile distribution of 10 m wind speed at all DWD stations for all

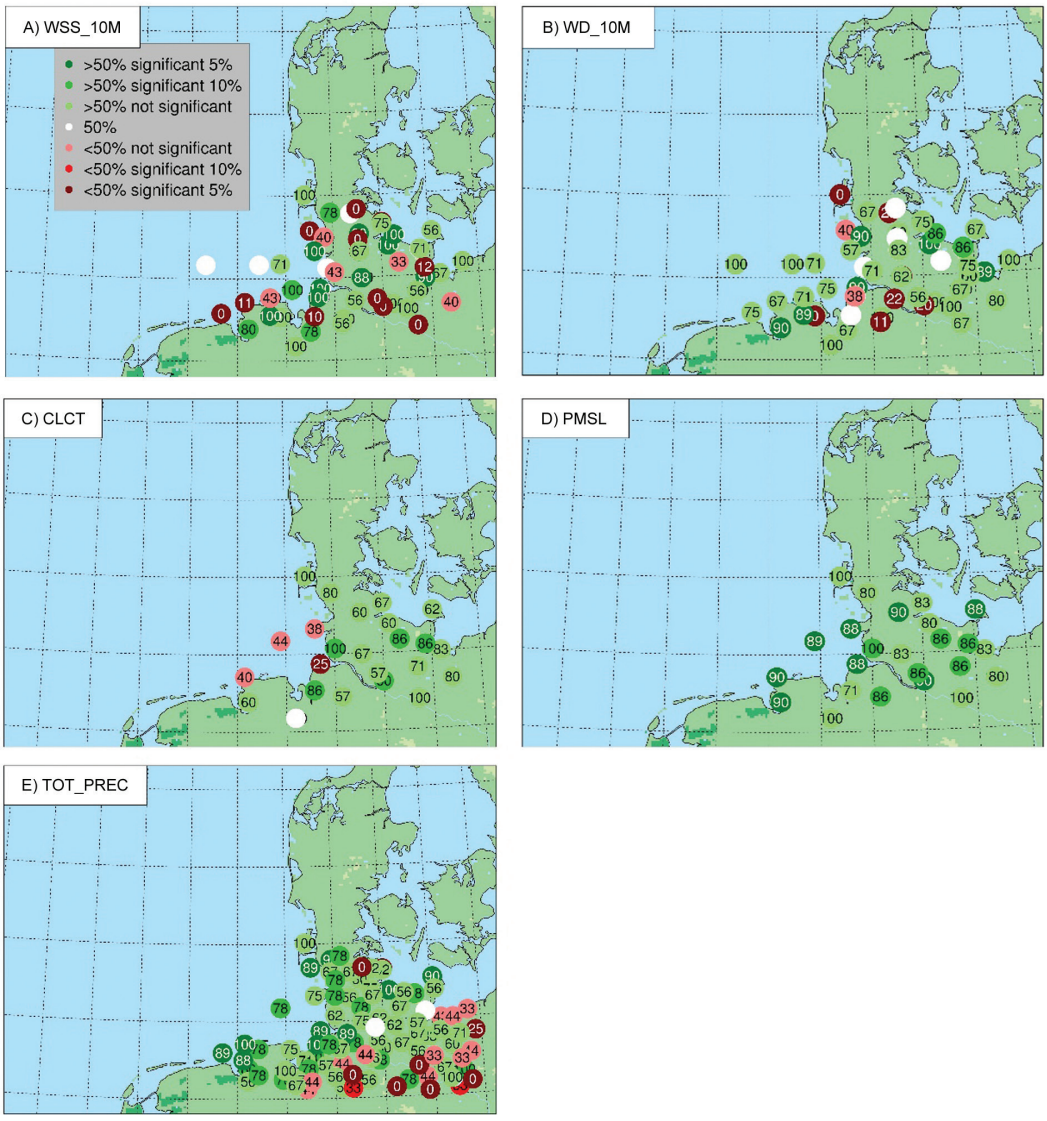

Fig. 8. Sign test for *BSS* between CCLM028 and CCLM240 in comparison to DWD station data for all 10 storms at all available DWD stations for the variables: a) wind speed (WSS), b) wind direction (WD), c) total cloud cover (CLCT), d) mean sea level pressure (PMSL), and e) total precipitation (TOT_PREC); shown is the percentage of storm cases with a *BSS* larger than 0, which indicates an added value of CCLM028 compared with CCLM240; green dots show that more than 50% of all storm cases which were measured at an individual station have a positive *BSS*, white dots illustrate that 50% of the storm cases have a positive *BSS*, and red dots represent values of less than 50%; the numbers in the dots give the percentage of positive *BSS* values; light colours indicate that the sign test at a station is not significant according to a significance test; thereby very light colours represent stations where the sign test was not significant at the 10% significance level; medium-light colours show stations where the sign test was significant at the 10% level, but not at the 5% significance level

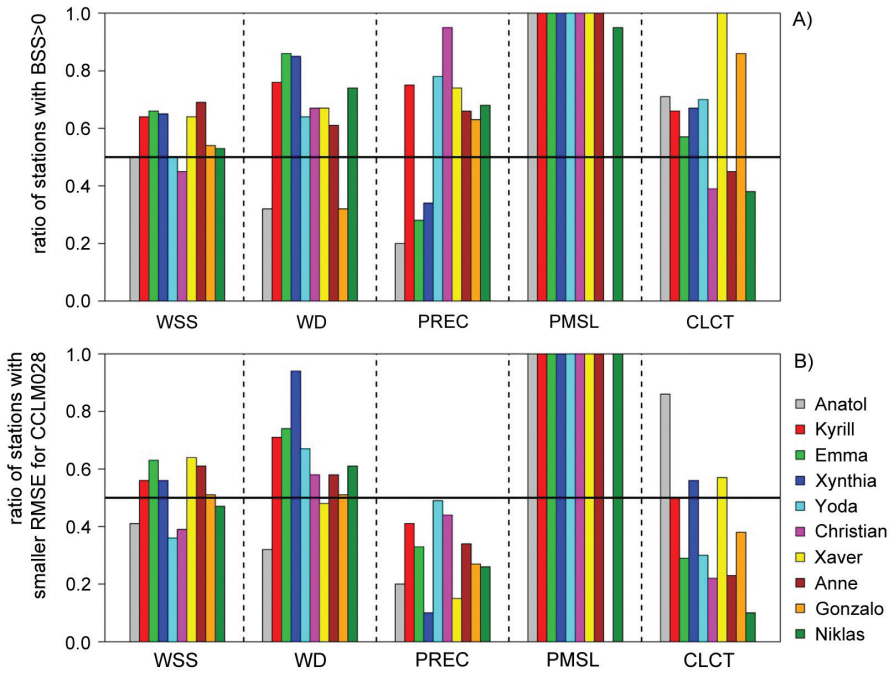

Fig. 9. Ratio of stations with a Brier Skill Score larger than 0 (a) and smaller *RMSE* for CCLM028 (b) for all storm cases and variables: WSS: wind speed, WD: wind direction, PREC: precipitation, PMSL: mean sea level pressure, CLCT: total cloud cover

Tab. 4. 10 m wind speed bias [m/s] averaged over all stations and time correlation (T.C.) of CCLM028 and CCLM240 for the ten storm events

	Anatol	Kyrill	Emma	Xynthia	Yoda	Christian	Xaver	Anne	Gonzalo	Niklas
Bias CCLM028	–1.05	0.17	0.98	0.38	0.20	0.06	-0.01	0.75	0.25	–0.47
Bias CCLM240	0.09	0.87	1.50	0.62	0.57	0.78	0.66	1.17	0.59	–0.20
T.C. CCLM028	0.75	0.77	0.82	0.69	0.83	0.34	0.90	0.64	0.26	0.17
T.C. CCLM240	0.79	0.77	0.83	0.67	0.86	0.50	0.91	0.65	0.30	0.18

ten storm cases. The 99 dots per colour represent the wind speed percentiles in steps of 1 percent from the 1st to the 99th percentile. Both models are close to the observations except for the highest wind speeds. For low wind speeds up to about 10 m/s, CCLM028 is closer to observed wind speeds than CCLM240, which shows slightly higher values. For wind speeds larger than 15 m/s, both models show smaller values than the observations. For CCLM028, the values are even smaller, and for the most extreme wind speeds they converge towards CCLM240. This difference between both models for higher wind speeds will be examined in more detail in the following chapter, which takes a closer look at the roughness length of both simulations.

The 10 m wind speed *RMSE* between modelled and observed 10 m wind speed was analyzed for all 34 DWD stations available. For most storm cases the majority of stations showed a smaller *RMSE* for CCLM028 and thus an added value for the high-resolution simulation (Fig. 9). The 10 m wind speed bias and time correlation in Tab. 4 show that there is an added value for CCLM028 for the bias (mean over all stations) for most storm events. The time correlation is not improved with higher resolution except for storm Xynthia, but the values are close to the ones of CCLM240.

3.2.2. Impact of roughness length in the high-resolution

Since both RCM simulations differ for the higher wind speeds (as presented in Fig. 10), we examine the roughness length in both models, which is one of the main factors to influence modelled near-surface wind speed. As already presented in Chapter 3.2, Fig. 6 shows the time series of wind speed during storm Christian (October 28 to 30, 2013) at a buoy in the North Sea and for the station Hamburg airport. Over the North Sea, both models are close to each other and to the observations, except for the largest peak on October 28 which is underestimated by the RCMs. However, the time series for the city of Hamburg (Fig. 6) show systematically lower values for the high-resolution simulation. This different behavior of the RCMs at urban and sea stations can be explained by differing roughness length values. Figure 11 shows that the urban

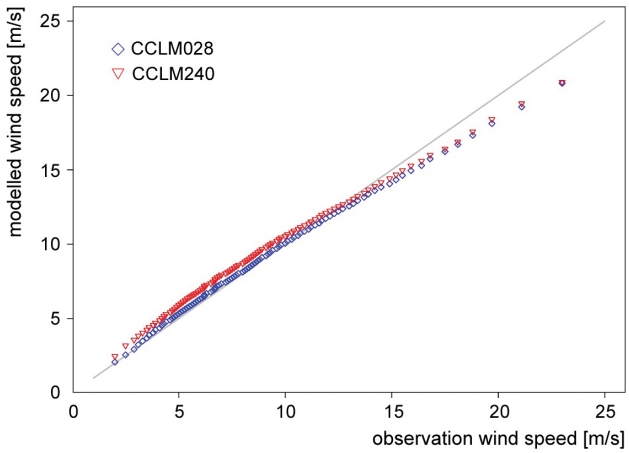

Fig. 10. Mean percentile-percentile distribution of 10 m wind speed averaged across all DWD stations and grid points of the DWD stations for all ten storm cases; 99 dots per colour represent the wind speed percentiles in steps of 1 percent from the 1st to the 99th percentile of all storm events

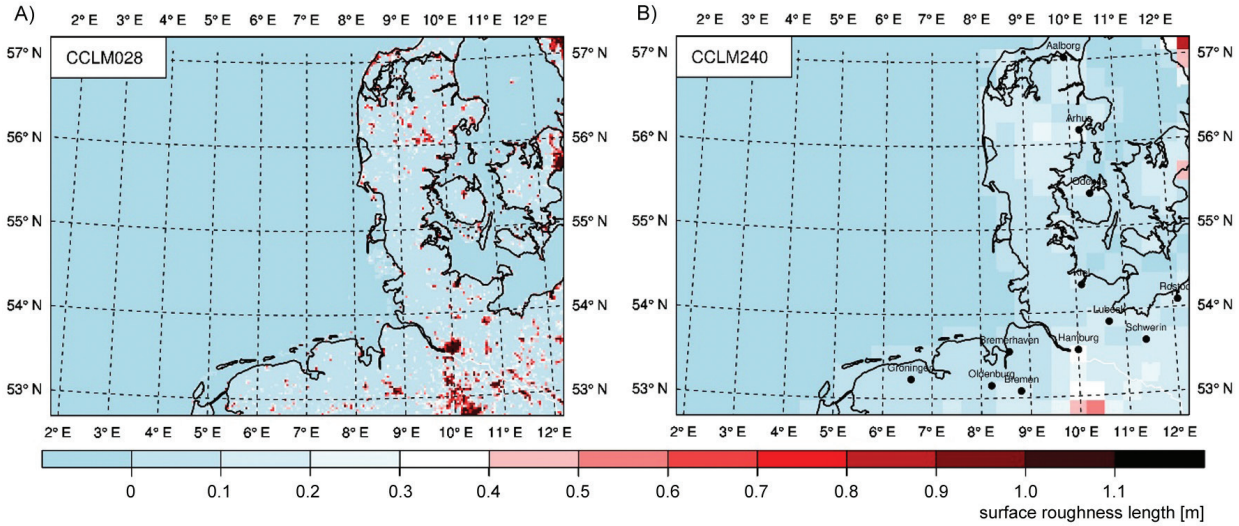

Fig. 11. Roughness length [m] in a) the CCLM028 and b) the CCLM240 model domain; the 12 largest cities in the model domain are marked in Fig. 11b

areas of CCLM028 feature larger roughness length values than CCLM240. Also the hilly area south of Hamburg and the hills in the middle of Denmark have larger roughness lengths. The 99th wind speed percentile difference between CCLM028 and CCLM240 (Fig. 12) shows lower extreme wind speeds (selected from mean hourly wind speeds) over the cities for the CCLM028 simulation. The high roughness length values and according low near-surface wind speeds of the convection-permitting simulation pose a potential problem for comparison with observation data. Normally weather stations are built in open-space areas surrounded by as few obstacles as possible, but nevertheless close to the city centre, e.g., at an airport. The roughness length in this flat countryside is not representative for the adjacent city areas, where more dense construction can be found and thus higher roughness length values prevail. The results therefore suggest an underestimation of the CCLM028 near-surface wind speeds in urban areas in

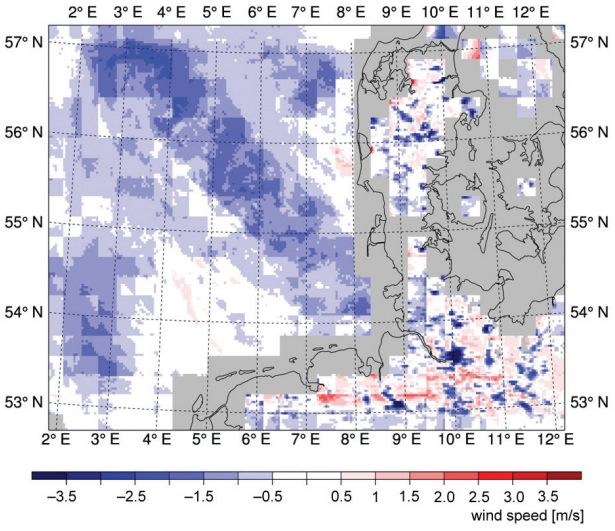

Fig. 12. Difference of the 99th wind speed percentile between CCLM028 and CCLM240 for all ten storm events; grey areas mark regions which are land points in CCLM028 and sea points in CCLM240 or vice versa

comparison to observations, even though they are presumably more representative for cities than the coarser RCM simulation.

4. Summary and conclusions

This study analyzed if convection-permitting high-resolution RCM simulations can provide an added value for strong storm and high wind conditions in comparison to RCM runs which use parameterized convection. The convective-permitting simulations were carried out with the RCM CCLM (Steppeler et al. 2003; Rockel et al. 2008) with a grid distance of 2.8 km (CCLM028) for Northern Germany and the German Bight, forced by a coarser (about 24 km grid point distance) CCLM simulation (Geyer 2014). Ten high-impact storm events between 1999 and 2013 were selected and examined for potential added value of CCLM028 in comparison to CCLM240.

Winter storm Christian of October 2013 was discussed in more detail to show small-scale meteorological features of the high-resolution simulation. For this storm, the high-resolution CCLM028 simulation shows more convective and more intense precipitation at its cold front in comparison to the CCLM240 simulation, which could not resolve these small-scale patterns. The convective precipitation is produced by deep convective cumulus cloud, which is produced explicitly with CCLM028. The precipitation is not so intense if it is produced with the deep convective parametrization used in CCLM240. Behind the cold front, post-frontal subsidence and partly clear skies were simulated by CCLM028 in contrast to the coarser simulation. The grid distance of CCLM240 is too small to show this small band of cloud-free area because the descending motion of the air mass is restricted too locally. The regionally simulated wind speeds for storm Christian are lower than the observed ones. A Brier Skill Score analysis for storm Christian between the regional simulations and DWD station data as a reference was computed at all stations. The largest added value for CCLM028 was found for mean sea level pressure and precipitation, followed by wind direction, but generally the *BSS* values were small. For wind speed and total cloud cover, both RCM data sets are of about the same quality.

Statistical analysis, such as the Brier Skill Score or a sign test of the 10 storm events, showed an added value for the high-resolution RCM simulation compared to the coarser simulation for many variables. Added value could be seen here for mean sea level pressure, wind speed, precipitation, wind direction, and cloud cover, but again the *BSS* values were small and therefore not as distinct to show added value as the synoptic comparisons.

A wind speed percentile-percentile distribution revealed an added value for lower wind speeds up to about 15 m/s for CCLM028 in comparison to CCLM240. For higher wind speeds, CCLM240 is slightly closer to the observations, while both RCMs show an underestimation of the most extreme wind speeds. These differences are most pronounced over urban areas, while both RCMs show very similar wind speeds over topographically flat regions like the North Sea. Such different behavior arises from varying roughness length values between both RCM runs. A more detailed roughness length, especially in urban areas, is a potential advantage of the higher resolution, but makes the comparison with meteorological weather stations more difficult. This is due to the fact that many urban stations are not representative for densely built cities, even if they are located close to the city centres. However, the prescribed model roughness length of the convective-permitting simulation could still be improved. The whole city area shows high roughness length values greater than 1, even for areas that should have lower roughness lengths, like airports and fields, which should be resolved at this resolution.

This study revealed that convection-permitting RCM simulations can add value to coarser RCM simulations for high wind and storm conditions over the German Bight and Northern Germany in terms of synoptic comparisons such as the analysis of frontal systems. Here, the higher resolution gives more realistic results for frontal mesoscale precipitation patterns or post-frontal cloud structures. More general statistical measures, such as the *BSS* or *RMSE*, provided less clear results in terms of added value for this study. This is in agreement with Di Luca et al. (2012) who suggest that exploring particular weather events may be more meaningful than statistical evaluations to detect added value. Long-term simulations covering more storm cases and using different model domains – in size and geographical location – would provide a valuable addition to our results and are planned as future work.

Acknowledgements

The work was supported through the Cluster of Excellence ‘CliSAP’ (EXC177), Universität Hamburg, funded through the German Research Foundation (DFG). It is a contribution to the Helmholtz Climate Initiative REKLIM (Regional Climate Change), a joint research project of the Helmholtz Association of German research centres (HGF). The CCLM is the community model of German climate research (www.clm-community.eu). The German Climate Computing Center (DKRZ) provided the computer hardware for the regional climate model simulations in the project ‘Storms’. We thank Hans

von Storch and Felix Ament for their valuable comments and suggestions regarding this study. Burkhardt Rockel, Eduardo Zorita, Markus Schultze and Delei Li provided helpful discussions. We are grateful to Beate Geyer for the CoastDat II data set. We thank Ingo Lange from the Meteorological Institute of the University of Hamburg for the provision of the data from the Wettermast Hamburg station. The German Weather Service (DWD) supplied measurement data and storm track analyses. We would like to thank Dennis Bray for proofreading this paper. Ingeborg Nöhren helped with the preparation of the Figures for this paper.

Bibliography

Baldauf M., Seifert A., Förstner J., Majewski D., Raschendorfer M., Reinhardt T., 2011, Operational convective-scale numerical weather prediction with the COSMO model: description and sensitivities, Monthly Weather Review, 139 (12), 3887-3905, DOI: 10.1175/MWR-D-10-05013.1

Chan S.C., Kendon E.J., Fowler H.J., Blenkinsop S., Roberts N.M, Ferro C.A., 2014, The value of high-resolution Met Office Regional Climate Models in the simulation of multihourly precipitation extremes, Journal of Climate, 27 (16), 6155-6174, DOI: 10.1175/JCLI-D-13-00723.1

Cholette M., Laprise R., Thériault J.M., 2015, Perspectives for very high-resolution climate simulations with nested models: illustration of potential in simulating St. Lawrence River Valley channelling winds with the fifth-generation Canadian Regional Climate Model, Climate, 3 (2), 283-307, DOI: 10.3390/cli3020283

Di Luca A., Argüeso D., Evans J.P., de Elía R., Laprise R., 2016, Quantifying the overall added value of dynamical downscaling and the contribution from different spatial scales, Journal of Geophysical Research Atmospheres, 121 (4), DOI: 10.1002/2015JD024009

Di Luca A., de Elía R., Laprise R., 2012, Potential for added value in precipitation simulated by high-resolution nested Regional Climate Models and observations, Climate Dynamics, 38 (5-6), 1229-1247, DOI: 10.1007/s00382-011-1068-3

Di Luca A., de Elía R., Laprise R., 2015, Challenges in the quest for added value of regional climate dynamical downscaling, Current Climate Change Reports, 1 (1), 10-21, DOI: 10.1007/s40641-015-0003-9

Feser F., Barcikowska M., Krueger O., Schenk F., Weisse R., Xia L., 2015, Storminess over the North Atlantic and Northwestern Europe – a review, Quarterly Journal of the Royal Meteorological Society, 141 (687), 350-382, DOI: 10.1002/qj.2364

Feser F., Rockel B., von Storch H., Winterfeldt J., Zahn M., 2011, Regional climate models add value to global model data: a review and selected examples, Bulletin of the American Meteorological Society, 92 (9), 1181-1192, DOI: 10.1175/2011BAMS3061.1

Feser F., von Storch H., 2005, A spatial two-dimensional discrete filter for limited-area-model evaluation purposes, Monthly Weather Review, 133 (6), 1774-1786, DOI: 10.1175/MWR2939.1

Feser F., von Storch H., 2008, A dynamical downscaling case study for typhoons in SE Asia using a Regional Climate Model, Monthly Weather Review, 136 (5), 1806-1815, DOI: 10.1175/2007MWR2207.1

Gallagher S., Tiron R., Whelan E., Gleeson E., Dias F., McGrath R., 2016, The nearshore wind and wave energy potential of Ireland: a high resolution assessment of availability and accessibility, Renewable Energy, 88, 494-516, DOI: 10.1016/j.renene.2015.11.010

Gentry M.S., Lackmann G.S., 2010, Sensitivity of simulated tropical cyclone structure and intensity to horizontal resolution, Monthly Weather Review, 138, 688-704, DOI: 10.1175/2009MWR2976.1

Geyer B., 2014, High-resolution atmospheric reconstruction for Europe 1948-2012: coastDat2, Earth System Science Data, 6, 147-164, DOI: 10.5194/essd-6-147-2014

Geyer B., Rockel B., 2013, coastDat-2 COSMO-CLM, available at: http://cera-www.dkrz.de/WDCC/ui/Compact.jsp?acronym=coastDat-2_COSMO-CLM (data access 20.02.2018)

Haeseler B., Lefebvre C., 2013, Heavy storm CHRISTIAN on 28 October 2013, available at: http://www.dwd.de/bvbw/generator/DWDWWW/Content/Oeffentlichkeit/KU/KU2/KU24/besondere__ereignisse__global/stuerme/englische-berichte/20131028__CHRISTIAN__europe,templateId=raw,property=publicationFile.pdf/20131028_CHRISTIAN_europe.pdf (data access 20.02.2018)

Kain J.S., Weiss S.J., Levit J.J., Baldwin M.E., Bright D.R., 2006, Examination of convection-allowing configurations of the WRF model for the prediction of severe convective weather: the SPC/NSSL Spring Program 2004, Weather Forecasting, 21 (2), 167-181, DOI: 10.1175/WAF906.1

Kalnay E., Kanamitsu M., Kistler R., Collins W., Deaven D., Gandin L., Iredell M., Saha S., White G., Woollen J., Zhu Y., Leetmaa A., Reynolds B., Chelliah M., Ebisuzaki W., Higgins W., Janowiak J., Mo K.C., Ropelewski C., Wang J., Roy J., Dennis J., 1996, The NCEP/NCAR 40-year reanalysis project, Bulletin of the American Meteorological Society, 77 (3), 437-471, DOI: 10.1175/1520-0477(1996)077<0437:TNYRP>2.0.CO;2

Klawa M., Ulbrich U., 2003, A model for the estimation of storm losses and the identification of severe winter storms in Germany, Natural Hazards and Earth System Sciences, 3, 725-732, DOI: 10.5194/nhess-3-725-2003

Lange I., 2014, Wind- und Temperaturdaten vom Wettermast Hamburg des Meteorologischen Instituts der Universität Hamburg, pers., com.

Li D., von Storch H., Geyer B., 2016, High-resolution wind hindcast over the Bohai Sea and the Yellow Sea in East Asia: evaluation and wind climatology analysis, Journal of Geophysical Research, 121 (1), 111-129, DOI: 10.1002/2015JD024177

Liberato M.L.R., Pinto J.G., Trigo R.M., Ludwig P., Ordóñez P., Yuen D., Trigo I.F., 2013, Explosive development of winter storm Xynthia over the Southeastern North Atlantic Ocean, Natural Hazards and Earth System Sciences, 13, 2239-2251, DOI: 10.5194/nhess-13-2239-2013

Ludwig P., Pinto J.G., Hoepp S.A., Fink A.H., Gray S.L., 2015, Secondary cyclogenesis along an occluded front leading to damaging wind gusts: windstorm Kyrill, January 2007, Monthly Weather Review, 143 (4), 1417-1437, DOI: 10.1175/MWR-D-14-00304.1

Neumayer E., Barthel F., 2011, Normalizing economic loss from natural disasters: a global analysis, Global Environmental Change, 21 (1), 13-24, DOI: 10.1016/j.gloenvcha.2010.10.004

Nilsson C., Goyette S., Barring L., 2007, Relating forest damage data to the wind field from high-resolution RCM simulations: case study of Anatol striking Sweden in December 1999, Global and Planetary Change, 57 (1-2), 161-176, DOI: 10.1016/j.gloplacha.2006.11.011

Parker R.J., Reich B.J., Sain S.R., 2015, A multiresolution approach to estimating the value added by regional climate models, Journal of Climate, 28 (22), 8873-8887, DOI: 10.1175/JCLI-D-14-00557.1

Pinto J.G., Fröhlich E.L., Leckebusch G.C., Ulbrich U., 2007, Changing European storm loss potentials under modified climate conditions according to ensemble simulations of the ECHAM5/MPI-OM1 GCM, Natural Hazards and Earth System Sciences, 7 (1), 165-175, DOI: 10.5194/nhess-7-165-2007

Prein A.F., Gobiet A., Suklitsch M., Truhetz H., Awan N.K., Keuler K., Georgievski G., 2013, Added value of convection permitting seasonal simulations, Climate Dynamics, 41 (9-10), 26555-262677, DOI: 10.1007/s00382-013-1744-6

Prein A.F., Langhans W., Fosser G., Ferrone A., Ban N., Goergen K., Keller M., Tölle M., Gutjahr O., Feser F., Brisson E., Kollet S., Schmidli J., van Lipzig N.M.P., Leung R., 2015, A review on regional convection-permitting climate modeling: demonstrations, prospects, and challenges, Reviews of Geophysics, 53 (2), 323-361, DOI: 10.1002/2014RG000475

Rockel B., Will A., Hense A., 2008, The Regional Climate Model COSMO-CLM (CCLM), Meteorologische Zeitschrift, 17 (4), 347-348, DOI: 10.1127/0941-2948/2008/0309

Schaaf B., von Storch H., Feser F., 2017, Does spectral nudging have an effect on dynamical downscaling applied in small regional model domains?, Monthly Weather Review, 145 (10), 4303-4311, DOI: 10.1175/MWR-D-17-0087.1

Schulz J.-P., 2008, Revision of the turbulent gust diagnostic in the COSMO model, COSMO Newsletter, 8, 17-22

Schulz J.-P., Heise E., 2003, A new scheme for diagnosing near-surface convective gusts, COSMO Newsletter, 3, 221-225

Shapiro M.A., Keyser D., 1990, Fronts, jet streams and the tropopause, [in:] Extratropical Cyclones: the Erik Palmen Memorial Volume, C.W. Newton, E.O. Holopainen (eds.), American Meteorological Society, 167-191

Steppeler J., Doms G., Schättler U., Bitzer H.W., Gassmann A., Damrath U., Gregoric G., 2003, Meso-gamma scale forecasts using the nonhydrostatic model LM, Meteorology Atmospheric Physics, 82 (1-4), 75-96, DOI: 10.1007/s00703-001-0592-9

von Storch H., Feser F., Haeseler S., Lefebvre C., Stendel M., 2014, A violent midlatitude storm in Northern Germany and Denmark, 28 October 2013, [in:] Explaining extreme events of 2013 from a climate perspective, S.C. Herring, M.P. Hoerling, T.C. Peterson, P.A. Scott (eds.), Special supplement to the Bulletin of the American Meteorological Society, 95 (9), 76-78

von Storch H., Langenberg H., Feser F., 2000, A spectral nudging technique for dynamical downscaling purposes, Monthly Weather Review, 128 (10), 3664-3673, DOI: 10.1175/1520-0493(2000)128<3664:ASNTFD>2.0.CO;2

von Storch H., Zwiers F.W., 2002, Statistical analysis in climate research, Cambridge University Press, Cambridge, 496 pp.

Taraphdar S., Mukhopadhyay P., Leung L.R., Zhang F., Abhilash S., Goswami B.N., 2014, The role of moist processes in the intrinsic predictability of Indian Ocean cyclones, Journal of Geophysical Research: Atmospheres, 119 (13), 8032-8048, DOI: 10.1002/2013JD021265

Tiedtke M., 1989, A comprehensive mass flux scheme for cumulus parameterization in large-scale models, Monthly Weather Review, 117 (8), 1779-1800, DOI: 10.1175/1520-0493(1989)117<1779:ACMFSF>2.0.CO;2

Usbeck T., Waldner P., Dobbertin M., Ginzler C., Hoffmann C., Sutter F., Steinmeier C., Volz R., Schneiter G., Rebetez M., 2012, Relating remotely sensed forest damage data to wind data: storms Lothar (1999) and Vivian (1990) in Switzerland, Theoretical and Applied Climatology, 108 (3-4), 451-462, DOI: 10.1007/s00704-011-0526-5

Weisse R., Gaslikova L., Geyer B., Groll N., Meyer E., 2014, coastDat – model data for science and industry, Die Küste, 81, 5-18

Weisse R., von Storch H., Callies U., Chrastansky A., Feser F., Grabemann I., Günther H., Pluess A., Stoye T., Tellkamp J., Winterfeldt J., Woth K., 2009, Regional meteorological-marine reanalyses and climate change projections, Bulletin

of the American Meteorological Society, 90 (6), 849-860, DOI: 10.1175/2008BAMS2713.1

Weisse R., von Storch H., Feser F., 2005, Northeast Atlantic and North Sea storminess as simulated by a Regional Climate Model during 1958-2001 and comparison with observations, Journal of Climate, 18 (3), 465-479, DOI: 10.1175/JCLI-3281.1

Winterfeldt J., Geyer B., Weisse R., 2010, Using QuikSCAT in the added value assessment of dynamically downscaled wind speed, International Journal of Climatology, 31 (7), 1028-1039, DOI: 10.1002/joc.2105

Winterfeldt J., Weisse R., 2009, Assessment of value added for surface marine wind speed obtained from two regional climate models, Monthly Weather Review, 137 (9), 2955-2965, DOI: 10.1175/2009MWR2704.1

Xue M., Schleif J., Kong F., Thomas K.W., Wang Y., Zhu F., 2013, Track and intensity forecasting of hurricanes: impact of convection-permitting resolution and global ensemble Kalman filter analysis on 2010 Atlantic season forecasts, Weather Forecasting, 28, 1366-1384, DOI: 10.1175/WAF-D-12-00063.1